Article

Journal of Vibration and Control
1–13

DOI: 10.1177/1077546317734083
journals.sagepub.com/home/jvc
SAGE

Vibration analysis of nonlocal strain gradient embedded single-layer graphene sheets under nonuniform in-plane loads

Farzad Ebrahimi[1] and Mohammad Reza Barati[2]

Abstract

This paper develops a nonlocal strain gradient plate model for vibration analysis of graphene sheets under nonuniform in-plane mechanical loads. For more accurate analysis of graphene sheets, the proposed theory contains two scale parameters related to the nonlocal and strain gradient effects. Graphene sheet is modeled via a two-variable shear deformation plate theory needless of shear correction factors. Governing equations of a nonlocal strain gradient graphene sheet on elastic substrate are derived via Hamilton's principle. Galerkin's method is implemented to solve the governing equations for different boundary conditions. Effects of different factors such as in-plane loading, load factor, nonlocal parameter, length scale parameter, elastic foundation, and boundary conditions on vibration characteristics of graphene sheets are examined.

Keywords

Free vibration, refined plate theory, graphene sheets, nonlocal strain gradient, in-plane nonuniform load

1. Introduction

Graphene is an actually two-dimensional atomic crystal with exceptional electronic and mechanical properties. Many carbon based nanostructures including carbon nanotubes, nanoplates and nanobeams are considered as deformed graphene sheets. In fact, analysis of graphene sheets is a basic matter in the study of the nanomaterials and nanostructures. Analysis of scale-free plates has been performed widely in the literature employing classical theories. But, such theories are not able to examine the scale effects on the nanostructures with small size. Therefore, the nonlocal elasticity theory of Eringen and Edelen (1972) and Eringen (1983) is developed taking into account small scale effects. Contrary to the local theory in which the stress state at any given point depends only on the strain state at that point, in the nonlocal theory, the stress state at a given point depends on the strain states at all points. The nonlocal elasticity theory has been broadly applied to investigate the mechanical behavior of nanoscale structures (Ebrahimi and Barati, 2016a, 2016b, 2016c, 2016d).

Pradhan and Murmu (2009) examined nonlocal influences on buckling behavior of a single-layer graphene sheet subjected to uniform in-plane loadings. Also, Pradhan and Kumar (2011) performed a vibration study of orthotropic graphene sheets incorporating nonlocal effects using a semi-analytical approach. Application of the Levy type method in stability and vibrational investigation of nanosize plates including nonlocal effects is examined by Aksencer and Aydogdu (2011). Mohammadi et al. (2014) performed shear buckling analysis of an orthotropic graphene sheet on elastic substrate including thermal loading effect. In another work, Mohammadi et al. (2013) examined the effect of in-plane loading on nonlocal vibrational behavior of circular graphene sheets. Also, Ansari et al. (2011) explored the vibration response of embedded nonlocal multi-layered graphene sheets

[1]Department of Mechanical Engineering, Faculty of Engineering, Imam Khomeini International University, Qazvin, Iran
[2]Aerospace Engineering Department & Center of Excellence in Computational Aerospace, AmirKabir University of Technology, Tehran, Iran

Received: 15 December 2016; accepted: 21 August 2017

Corresponding author:
Farzad Ebrahimi, Norozian Avenue, Qazvin 3414896818, Islamic Republic of Iran.
Email: febrahimy@eng.ikiu.ac.ir

accounting for various boundary conditions. Shen et al. (2012) studied vibration behavior of a nanomechanical mass sensor based on the nonlocal graphene sheet model. They showed that the vibration response of a graphene sheet is significantly influenced by the mass of the attached nanoparticle. Farajpour et al. (2012) examined static stability of nonlocal plates subjected to nonuniform in-plane edge loads. Also, Ansari and Sahmani (2013) employed molecular dynamics simulations to examine biaxial buckling behavior of single-layered graphene sheets based on nonlocal elasticity theory. They matched the results obtained by molecular dynamics simulations with those of a nonlocal plate model to extract the appropriate values of the nonlocal parameter. Static bending and vibrational behavior of single-layered graphene sheets on a Winkler–Pasternak foundation based on a two-variable higher order shear deformation theory is studied by Sobhy (2014). Also, Narendar and Gopalakrishnan (2012) carried out size-dependent stability analysis of orthotropic nanoscale plates according to a nonlocal two-variable refined plate theory. They stated that the two-variable refined plate model considers the transverse shear influences through the thickness of the plate, hence, it is unnecessary to apply shear correction factors. Murmu et al. (2013) explored the influence of unidirectional magnetic fields on vibrational behavior of nonlocal single-layer graphene sheets resting on elastic substrate. Bessaim et al. (2015) presented a nonlocal quasi-three-dimensional trigonometric plate model for free vibration behavior of micro/nanoscale plates. Hashemi et al. (2015) studied free vibrational behavior of double viscoelastic graphene sheets coupled by a visco-Pasternak medium. Jiang et al. (2016) conducted vibration analysis of a single-layered graphene sheet-based mass sensor using the Galerkin strip distributed transfer function method. Arani et al. (2016) examined nonlocal vibration of an axially moving graphene sheet resting on orthotropic a visco-Pasternak foundation under a longitudinal magnetic field. Sobhy (2016) analyzed the hygro-thermal vibrational behavior of coupled graphene sheets by an elastic medium using the two-variable plate theory. Also, Zenkour (2016) performed transient thermal analysis of graphene sheets on a viscoelastic foundation based on nonlocal elasticity theory. Zhang et al. (2016a) examined free vibrational behavior of magnetically affected bilayer graphene sheets.

Application of nonlocal elasticity theory in modeling and simulation of graphene sheets is examined by Liew et al. (2017). It is clear that all of the previous papers on graphene sheets applied only the nonlocal elasticity theory to capture small scale effects. However, nonlocal elasticity theory has some limitations in accurate prediction of mechanical behavior of nanostructures, because nonlocal elasticity theory is unable to examine the stiffness increment observed in experimental works and strain gradient elasticity (Lam et al., 2003; Yan et al., 2015). Recently, Lim et al. (2015) proposed the nonlocal strain gradient theory to introduce both of the length scales into a single theory. The nonlocal strain gradient theory captures the true influence of the two length scale parameters on the physical and mechanical behavior of small size structures (Li et al., 2016a, 2016b). Recently, Ebrahimi and Barati (2016e, 2016f, 2017a, 2017b) applied the nonlocal strain gradient theory in analysis of nanobeams. They mentioned that mechanical characteristics of nanostructures are significantly affected by stiffness-softening and stiffness-hardening mechanisms due to the nonlocal and strain gradient effects, respectively. Most recently, Ebrahimi et al. (2016) extended the nonlocal strain gradient theory for analysis of nanoplates to obtain the wave frequencies for a range of two scale parameters. So, it is crucial to incorporate both nonlocal and strain gradient effects in analysis of graphene sheets.

Based on a newly developed nonlocal strain gradient theory, free vibration behavior of single-layer graphene sheets under in-plane loads resting on elastic medium is examined using a refined two-variable plate theory. The theory introduces two scale parameters corresponding to nonlocal and strain gradient effects to capture both stiffness-softening and stiffness-hardening influences. Hamilton's principle is employed to obtain the governing equation of a nonlocal strain gradient graphene sheet. These equations are solved via Galerkin's method to obtain the natural frequencies. It is shown that vibration behavior of graphene sheets is significantly influenced by the nonlocal parameter, length scale parameter, in-plane loading, load factor, elastic foundation, and boundary conditions.

2. Governing equations

The higher-order refined plate theory has the following displacement field as:

$$u_1(x,y,z) = -z\frac{\partial w_b}{\partial x} - f(z)\frac{\partial w_s}{\partial x} \tag{1}$$

$$u_2(x,y,z) = -z\frac{\partial w_b}{\partial y} - f(z)\frac{\partial w_s}{\partial y} \tag{2}$$

$$u_3(x,y,z) = w_b(x,y) + w_s(x,y) \tag{3}$$

where the present theory has a trigonometric function in the following form:

$$f(z) = z - \frac{h}{\pi}\sin\left(\frac{\pi z}{h}\right) \tag{4}$$

Also, w_b and w_s denote the bending and shear transverse displacement, respectively. Nonzero strains of the present plate model are expressed as follows:

$$\left\{\begin{array}{c}\varepsilon_x\\ \varepsilon_y\\ \gamma_{xy}\end{array}\right\}=z\left\{\begin{array}{c}\kappa_x^b\\ \kappa_y^b\\ \kappa_{xy}^b\end{array}\right\}+f(z)\left\{\begin{array}{c}\kappa_x^s\\ \kappa_y^s\\ \kappa_{xy}^s\end{array}\right\},\ \left\{\begin{array}{c}\gamma_{yz}\\ \gamma_{xz}\end{array}\right\}=g(z)\left\{\begin{array}{c}\gamma_{yz}^s\\ \gamma_{xz}^s\end{array}\right\} \tag{5}$$

where $g(z)=1-df/dz$ and

$$\left\{\begin{array}{c}\kappa_x^b\\ \kappa_y^b\\ \kappa_{xy}^b\end{array}\right\}=\left\{\begin{array}{c}-\frac{\partial^2 w_b}{\partial x^2}\\ -\frac{\partial^2 w_b}{\partial y^2}\\ -2\frac{\partial^2 w_b}{\partial x\partial y}\end{array}\right\},\ \left\{\begin{array}{c}\kappa_x^s\\ \kappa_y^s\\ \kappa_{xy}^s\end{array}\right\}=\left\{\begin{array}{c}-\frac{\partial^2 w_s}{\partial x^2}\\ -\frac{\partial^2 w_s}{\partial y^2}\\ -2\frac{\partial^2 w_s}{\partial x\partial y}\end{array}\right\},\quad \left\{\begin{array}{c}\gamma_{yz}^s\\ \gamma_{xz}^s\end{array}\right\}=\left\{\begin{array}{c}\frac{\partial w_s}{\partial y}\\ \frac{\partial w_s}{\partial x}\end{array}\right\} \tag{6}$$

Also, Hamilton's principle expresses that:

$$\int_0^t \delta(U-T+V)\,\mathrm{d}t=0 \tag{7}$$

in which U is strain energy, T is kinetic energy and V is work done by external loads. The variation of strain energy is calculated as:

$$\begin{aligned}\delta U=\int_v \sigma_{ij}\delta\varepsilon_{ij}\,\mathrm{d}V=\int_v(&\sigma_x\delta\varepsilon_x+\sigma_y\delta\varepsilon_y+\sigma_{xy}\delta\gamma_{xy}\\&+\sigma_{yz}\delta\gamma_{yz}+\sigma_{xz}\delta\gamma_{xz})\,\mathrm{d}V\end{aligned} \tag{8}$$

Substituting equations (5) and (6) into equation (8) yields:

$$\begin{aligned}\delta U=\int_0^b\int_0^a\Big[&-M_x^b\frac{\partial^2\delta w_b}{\partial x^2}-M_x^s\frac{\partial^2\delta w_s}{\partial x^2}\\&-M_y^b\frac{\partial^2\delta w_b}{\partial y^2}-M_y^s\frac{\partial^2\delta w_s}{\partial y^2}\\&-2M_{xy}^b\frac{\partial^2\delta w_b}{\partial x\partial y}-2M_{xy}^s\frac{\partial^2\delta w_s}{\partial x\partial y}\\&+Q_{yz}\frac{\partial\delta w_s}{\partial y}+Q_{xz}\frac{\partial\delta w_s}{\partial x}\Big]\mathrm{d}x\,\mathrm{d}y\end{aligned} \tag{9}$$

in which

$$\begin{aligned}(M_i^b,M_i^s)&=\int_{-h/2}^{h/2}(z,f)\sigma_i\,dz,\ i=(x,y,xy)\\ Q_i&=\int_{-h/2}^{h/2}g\sigma_i dz,\ i=(xz,yz)\end{aligned} \tag{10}$$

The variation of the work done by applied loads can be written as:

$$\begin{aligned}\delta V=\int_0^b\int_0^a\Big(&N_x^0\frac{\partial(w_b+w_s)}{\partial x}\frac{\partial\delta(w_b+w_s)}{\partial x}.\\&+N_y^0\frac{\partial(w_b+w_s)}{\partial y}\frac{\partial\delta(w_b+w_s)}{\partial y}\\&+2\delta N_{xy}^0\frac{\partial(w_b+w_s)}{\partial x}\frac{\partial(w_b+w_s)}{\partial y}\\&-k_w\delta(w_b+w_s)+k_p\delta(w_b+w_s)\Big)\mathrm{d}x\,\mathrm{d}y\end{aligned} \tag{11}$$

where N_x^0, N_y^0, N_{xy}^0 are in-plane applied loads; k_w and k_p are Winkler and Pasternak constants. The variation of the kinetic energy is calculated as:

$$\begin{aligned}\delta K=\int_0^b\int_0^a\Big[&I_0\left(\frac{\partial(w_b+w_s)}{\partial t}\frac{\partial\delta(w_b+w_s)}{\partial t}\right)\\&+I_2\left(\frac{\partial w_b}{\partial x\partial t}\frac{\partial\delta w_b}{\partial x\partial t}+\frac{\partial w_b}{\partial y\partial t}\frac{\partial\delta w_b}{\partial y\partial t}\right)\\&+K_2\left(\frac{\partial w_s}{\partial x\partial t}\frac{\partial\delta w_s}{\partial x\partial t}+\frac{\partial w_s}{\partial y\partial t}\frac{\partial\delta w_s}{\partial y\partial t}\right)\\&+J_2\left(\frac{\partial w_b}{\partial x\partial t}\frac{\partial\delta w_s}{\partial x\partial t}+\frac{\partial w_s}{\partial x\partial t}\frac{\partial\delta w_b}{\partial x\partial t}\right.\\&\left.+\frac{\partial w_b}{\partial y\partial t}\frac{\partial\delta w_s}{\partial y\partial t}+\frac{\partial w_s}{\partial y\partial t}\frac{\partial\delta w_b}{\partial y\partial t}\right)\Big]\mathrm{d}x\,\mathrm{d}y\end{aligned} \tag{12}$$

in which

$$(I_0,I_2,J_2,K_2)=\int_{-h/2}^{h/2}(1,z^2,\ zf,f^2)\rho\mathrm{d}z \tag{13}$$

By inserting equations (9)–(12) into equation (7) and setting the coefficients of δw_b and δw_s to zero, the following equations are obtained.

$$\begin{aligned}&\frac{\partial^2 M_x^b}{\partial x^2}+2\frac{\partial^2 M_{xy}^b}{\partial x\partial y}+\frac{\partial^2 M_y^b}{\partial y^2}-N_x^0(y)\frac{\partial^2(w_b+w_s)}{\partial x^2}\\&\quad-N_y^0(x)\frac{\partial^2(w_b+w_s)}{\partial y^2}\\&\quad+k_p\left[\frac{\partial^2(w_b+w_s)}{\partial x^2}+\frac{\partial^2(w_b+w_s)}{\partial y^2}\right]\\&\quad-k_w(w_b+w_s)=I_0\frac{\partial^2(w_b+w_s)}{\partial t^2}\\&\quad-I_2\nabla^2\left(\frac{\partial^2 w_b}{\partial t^2}\right)-J_2\nabla^2\left(\frac{\partial^2 w_s}{\partial t^2}\right)\end{aligned} \tag{14}$$

$$\begin{aligned}&\frac{\partial^2 M_x^s}{\partial x^2}+2\frac{\partial^2 M_{xy}^s}{\partial x\partial y}+\frac{\partial^2 M_y^s}{\partial y^2}+\frac{\partial Q_{xz}}{\partial x}+\frac{\partial Q_{yz}}{\partial y}\\&-N_x^0(y)\frac{\partial^2(w_b+w_s)}{\partial x^2}-N_y^0(x)\frac{\partial^2(w_b+w_s)}{\partial y^2}\\&+k_p\left[\frac{\partial^2(w_b+w_s)}{\partial x^2}+\frac{\partial^2(w_b+w_s)}{\partial y^2}\right]\\&-k_w(w_b+w_s)=I_0\frac{\partial^2(w_b+w_s)}{\partial t^2}\\&-J_2\nabla^2\left(\frac{\partial^2 w_b}{\partial t^2}\right)-K_2\nabla^2\left(\frac{\partial^2 w_s}{\partial t^2}\right)\end{aligned}\tag{15}$$

2.1. Nonlocal strain gradient nanoplate model

The newly developed nonlocal strain gradient theory by Ebrahimi et al. (2016) takes into account both nonlocal stress field and the strain gradient effects by introducing two scale parameters. This theory defines the stress field as:

$$\sigma_{ij}=\sigma_{ij}^{(0)}-\nabla\sigma_{ij}^{(1)}\tag{16}$$

in which the stresses $\sigma_{ij}^{(0)}$ and $\sigma_{ij}^{(1)}$ are corresponding to strain ε_{ij} and strain gradient $\nabla\varepsilon_{ij}$, respectively as:

$$\sigma_{ij}^{(0)}=\int_V C_{ijkl}\alpha_0(x,x',e_0a)\varepsilon'_{kl}(x')\mathrm{d}x'\tag{17a}$$

$$\sigma_{ij}^{(1)}=l^2\int_V C_{ijkl}\alpha_1(x,x',e_1a)\nabla\varepsilon'_{kl}(x')\mathrm{d}x'\tag{17b}$$

in which C_{ijkl} are the elastic coefficients and e_0a and e_1a capture the nonlocal effects and l captures the strain gradient effects. When the nonlocal functions $\alpha_0(x,x',e_0a)$ and $\alpha_1(x,x',e_1a)$ satisfy the developed conditions by Eringen (1983), the constitutive relation of nonlocal strain gradient theory has the following form (Ebrahimi et al., 2016):

$$\begin{aligned}&[1-(e_1a)^2\nabla^2][1-(e_0a)^2\nabla^2]\sigma_{ij}=C_{ijkl}[1-(e_1a)^2\nabla^2]\varepsilon_{kl}\\&-C_{ijkl}l^2[1-(e_0a)^2\nabla^2]\nabla^2\varepsilon_{kl}\end{aligned}\tag{18}$$

in which ∇^2 denotes the Laplacian operator. Considering $e_1=e_0=e$, the general constitutive relation in equation (18) becomes:

$$[1-(ea)^2\nabla^2]\sigma_{ij}=C_{ijkl}[1-l^2\nabla^2]\varepsilon_{kl}\tag{19}$$

Finally, the constitutive relations of nonlocal strain gradient theory can be expressed by:

$$\begin{aligned}&(1-\mu\nabla^2)\begin{Bmatrix}\sigma_x\\\sigma_y\\\sigma_{xy}\\\sigma_{yz}\\\sigma_{xz}\end{Bmatrix}=(1-\lambda\nabla^2)\\&\times\begin{pmatrix}Q_{11}&Q_{12}&0&0&0\\Q_{12}&Q_{22}&0&0&0\\0&0&Q_{66}&0&0\\0&0&0&Q_{44}&0\\0&0&0&0&Q_{55}\end{pmatrix}\begin{Bmatrix}\varepsilon_x\\\varepsilon_y\\\gamma_{xy}\\\gamma_{yz}\\\gamma_{xz}\end{Bmatrix}\end{aligned}\tag{20}$$

where

$$\begin{aligned}&Q_{11}=Q_{22}=\frac{E}{1-\upsilon^2},\ Q_{12}=\upsilon Q_{11},\\&Q_{44}=Q_{55}=Q_{66}=\frac{E}{2(1+\upsilon)}\end{aligned}\tag{21}$$

where $\mu=(ea)^2$ and $\lambda=l^2$. Inserting equation (10) in equation (23) gives:

$$\begin{aligned}&(1-\mu\nabla^2)\begin{Bmatrix}M_x^b\\M_y^b\\M_{xy}^b\end{Bmatrix}=(1-\lambda\nabla^2)\\&\times\left[\begin{pmatrix}D_{11}&D_{12}&0\\D_{12}&D_{22}&0\\0&0&D_{66}\end{pmatrix}\begin{Bmatrix}-\frac{\partial^2 w_b}{\partial x^2}\\-\frac{\partial^2 w_b}{\partial y^2}\\-2\frac{\partial^2 w_b}{\partial x\partial y}\end{Bmatrix}\right.\\&\left.+\begin{pmatrix}D_{11}^s&D_{12}^s&0\\D_{12}^s&D_{22}^s&0\\0&0&D_{66}^s\end{pmatrix}\begin{Bmatrix}-\frac{\partial^2 w_s}{\partial x^2}\\-\frac{\partial^2 w_s}{\partial y^2}\\-2\frac{\partial^2 w_s}{\partial x\partial y}\end{Bmatrix}\right]\end{aligned}\tag{22}$$

$$\begin{aligned}&(1-\mu\nabla^2)\begin{Bmatrix}M_x^s\\M_y^s\\M_{xy}^s\end{Bmatrix}=(1-\lambda\nabla^2)\\&\times\left[\begin{pmatrix}D_{11}^s&D_{12}^s&0\\D_{12}^s&D_{22}^s&0\\0&0&D_{66}^s\end{pmatrix}\begin{Bmatrix}-\frac{\partial^2 w_b}{\partial x^2}\\-\frac{\partial^2 w_b}{\partial y^2}\\-2\frac{\partial^2 w_b}{\partial x\partial y}\end{Bmatrix}\right.\\&\left.+\begin{pmatrix}H_{11}^s&H_{12}^s&0\\H_{12}^s&H_{22}^s&0\\0&0&H_{66}^s\end{pmatrix}\begin{Bmatrix}-\frac{\partial^2 w_s}{\partial x^2}\\-\frac{\partial^2 w_s}{\partial y^2}\\-2\frac{\partial^2 w_s}{\partial x\partial y}\end{Bmatrix}\right]\end{aligned}\tag{23}$$

$$(1-\mu\nabla^2)\begin{Bmatrix} Q_x \\ Q_y \end{Bmatrix} = (1-\lambda\nabla^2)\left[\begin{pmatrix} A^s_{44} & 0 \\ 0 & A^s_{55} \end{pmatrix}\begin{Bmatrix} \frac{\partial w_s}{\partial x} \\ \frac{\partial w_s}{\partial y} \end{Bmatrix}\right] \tag{24}$$

in which the cross-sectional rigidities are defined as follows:

$$\begin{Bmatrix} D_{11}, D^s_{11}, H^s_{11} \\ D_{12}, D^s_{12}, H^s_{12} \\ D_{66}, D^s_{66}, H^s_{66} \end{Bmatrix} = \int_{-h/2}^{h/2} Q_{11}\,(z^2,\ zf,f^2)\begin{Bmatrix} 1 \\ \upsilon \\ \frac{1-\upsilon}{2} \end{Bmatrix} dz \tag{25}$$

$$A^s_{44} = A^s_{55} = \int_{-h/2}^{h/2} g^2 \frac{E}{2(1+\upsilon)} dz \tag{26}$$

The governing equations of nonlocal strain gradient graphene sheet in terms of the displacement are obtained by inserting equations (25)–(27), into equations (14)–(15) as follows:

$$\begin{aligned}
&-D_{11}[\frac{\partial^4 w_b}{\partial x^4} - \lambda\left(\frac{\partial^6 w_b}{\partial x^6} + \frac{\partial^6 w_b}{\partial x^4 \partial y^2}\right)\Big] - 2(D_{12}+2D_{66}) \\
&\times\left[\frac{\partial^4 w_b}{\partial x^2 \partial y^2} - \lambda\left(\frac{\partial^6 w_b}{\partial x^4 \partial y^2} + \frac{\partial^6 w_b}{\partial x^2 \partial y^4}\right)\right] \\
&- D_{22}\left[\frac{\partial^4 w_b}{\partial y^4} - \lambda\left(\frac{\partial^6 w_b}{\partial y^6} + \frac{\partial^6 w_b}{\partial y^4 \partial x^2}\right)\right] \\
&- D^s_{11}\left[\frac{\partial^4 w_s}{\partial x^4} - \lambda\left(\frac{\partial^6 w_s}{\partial x^6} + \frac{\partial^6 w_s}{\partial x^4 \partial y^2}\right)\right] \\
&- 2(D^s_{12}+2D^s_{66})\left[\frac{\partial^4 w_s}{\partial x^2 \partial y^2} - \lambda\left(\frac{\partial^6 w_s}{\partial x^4 \partial y^2} + \frac{\partial^6 w_s}{\partial x^2 \partial y^4}\right)\right] \\
&- D^s_{22}\left[\frac{\partial^4 w_s}{\partial y^4} - \lambda\left(\frac{\partial^6 w_s}{\partial y^6} + \frac{\partial^6 w_s}{\partial y^4 \partial x^2}\right)\right] \\
&- I_0\left[\frac{\partial^2 (w_b+w_s)}{\partial t^2} - \mu\left(\frac{\partial^4 (w_b+w_s)}{\partial t^2 \partial x^2} + \frac{\partial^4 (w_b+w_s)}{\partial t^2 \partial y^2}\right)\right] \\
&+ I_2\left[\frac{\partial^4 w_b}{\partial x^2 \partial t^2} + \frac{\partial^4 w_b}{\partial y^2 \partial t^2} - \mu\left(\frac{\partial^6 w_b}{\partial t^2 \partial x^4}\right.\right. \\
&\left.\left. + 2\frac{\partial^6 w_b}{\partial t^2 \partial x^2 \partial y^2} + \frac{\partial^6 w_b}{\partial t^2 \partial y^4}\right)\right] + J_2\left[\frac{\partial^4 w_s}{\partial x^2 \partial t^2} + \frac{\partial^4 w_s}{\partial y^2 \partial t^2}\right. \\
&\left.-\mu\left(\frac{\partial^6 w_s}{\partial t^2 \partial x^4} + 2\frac{\partial^6 w_s}{\partial t^2 \partial x^2 \partial y^2} + \frac{\partial^6 w_s}{\partial t^2 \partial y^4}\right)\right] \\
&- N^0_x(y)\left[1-\mu\left(\frac{\partial^2}{\partial x^2} + \frac{\partial^2}{\partial y^2}\right)\right]\frac{\partial^2 (w_b+w_s)}{\partial x^2} \\
&- N^0_y(x)\left[1-\mu\left(\frac{\partial^2}{\partial x^2} + \frac{\partial^2}{\partial y^2}\right)\right]\frac{\partial^2 (w_b+w_s)}{\partial y^2} \\
&+ k_p\left[1-\mu\left(\frac{\partial^2}{\partial x^2} + \frac{\partial^2}{\partial y^2}\right)\right]\left[\frac{\partial^2 (w_b+w_s)}{\partial x^2} + \frac{\partial^2 (w_b+w_s)}{\partial y^2}\right] \\
&- k_w\left[(w_b+w_s) - \mu\left(\frac{\partial^2 (w_b+w_s)}{\partial x^2} + \frac{\partial^2 (w_b+w_s)}{\partial y^2}\right)\right] = 0
\end{aligned} \tag{27}$$

$$\begin{aligned}
&- D^s_{11}\left[\frac{\partial^4 w_b}{\partial x^4} - \lambda\left(\frac{\partial^6 w_b}{\partial x^6} + \frac{\partial^6 w_b}{\partial x^4 \partial y^2}\right)\right] \\
&+ A^s_{55}\left[\frac{\partial^2 w_s}{\partial x^2} - \lambda\left(\frac{\partial^4 w_s}{\partial x^4} + \frac{\partial^4 w_s}{\partial x^2 \partial y^2}\right)\right] \\
&+ A^s_{44}\left[\frac{\partial^2 w_s}{\partial y^2} - \lambda\left(\frac{\partial^4 w_s}{\partial y^4} + \frac{\partial^4 w_s}{\partial y^2 \partial x^2}\right)\right] \\
&- 2(D^s_{12}+2D^s_{66})\left[\frac{\partial^4 w_b}{\partial x^2 \partial y^2} - \lambda\left(\frac{\partial^6 w_b}{\partial x^4 \partial y^2} + \frac{\partial^6 w_b}{\partial x^2 \partial y^4}\right)\right] \\
&- D^s_{22}\left[\frac{\partial^4 w_b}{\partial y^4} - \lambda\left(\frac{\partial^6 w_b}{\partial y^6} + \frac{\partial^6 w_b}{\partial y^4 \partial x^2}\right)\right] \\
&- H^s_{11}\left[\frac{\partial^4 w_s}{\partial x^4} - \lambda\left(\frac{\partial^6 w_s}{\partial x^6} + \frac{\partial^6 w_s}{\partial x^4 \partial y^2}\right)\right] \\
&- 2(H^s_{12}+2H^s_{66})\left[\frac{\partial^4 w_s}{\partial x^2 \partial y^2} - \lambda\left(\frac{\partial^6 w_s}{\partial x^4 \partial y^2} + \frac{\partial^6 w_s}{\partial x^2 \partial y^4}\right)\right] \\
&- H^s_{22}\left[\frac{\partial^4 w_s}{\partial y^4} - \lambda\left(\frac{\partial^6 w_s}{\partial y^6} + \frac{\partial^6 w_s}{\partial y^4 \partial x^2}\right)\right] \\
&- I_0\left[\frac{\partial^2 (w_b+w_s)}{\partial t^2} - \mu\left(\frac{\partial^4 (w_b+w_s)}{\partial t^2 \partial x^2} + \frac{\partial^4 (w_b+w_s)}{\partial t^2 \partial y^2}\right)\right] \\
&+ J_2\left[\frac{\partial^4 w_b}{\partial x^2 \partial t^2} + \frac{\partial^4 w_b}{\partial y^2 \partial t^2} - \mu\left(\frac{\partial^6 w_b}{\partial t^2 \partial x^4}\right.\right. \\
&\left.\left. + 2\frac{\partial^6 w_b}{\partial t^2 \partial x^2 \partial y^2} + \frac{\partial^6 w_b}{\partial t^2 \partial y^4}\right)\right] + K_2\left[\frac{\partial^4 w_s}{\partial x^2 \partial t^2} + \frac{\partial^4 w_s}{\partial y^2 \partial t^2}\right. \\
&\left.-\mu\left(\frac{\partial^6 w_s}{\partial t^2 \partial x^4} + 2\frac{\partial^6 w_s}{\partial t^2 \partial x^2 \partial y^2} + \frac{\partial^6 w_s}{\partial t^2 \partial y^4}\right)\right] \\
&- N^0_x(y)\left[1-\mu\left(\frac{\partial^2}{\partial x^2} + \frac{\partial^2}{\partial y^2}\right)\right]\frac{\partial^2 (w_b+w_s)}{\partial x^2} \\
&- N^0_y(x)\left[1-\mu\left(\frac{\partial^2}{\partial x^2} + \frac{\partial^2}{\partial y^2}\right)\right]\frac{\partial^2 (w_b+w_s)}{\partial y^2} \\
&+ k_p\left[1-\mu\left(\frac{\partial^2}{\partial x^2} + \frac{\partial^2}{\partial y^2}\right)\right] \\
&\times\left[\frac{\partial^2 (w_b+w_s)}{\partial x^2} + \frac{\partial^2 (w_b+w_s)}{\partial y^2}\right] \\
&- k_w\left[(w_b+w_s) - \mu\left(\frac{\partial^2 (w_b+w_s)}{\partial x^2} + \frac{\partial^2 (w_b+w_s)}{\partial y^2}\right)\right] = 0
\end{aligned} \tag{28}$$

3. Solution by Galerkin's method

Up to now, several numerical solution methods are applied in analysis of small scale structures (Ansari et al., 2016; Zhang et al., 2015, 2016b, 2016c). In this section, Galerkin's method is implemented to solve the governing equations of nonlocal strain gradient graphene sheets. Thus, the displacement field can be calculated as:

$$w_b = \sum_{m=1}^{\infty}\sum_{n=1}^{\infty} W_{bmn}\Phi_{bm}(x)\Psi_{bn}(y)e^{i\omega_n t} \tag{29}$$

$$w_s = \sum_{m=1}^{\infty}\sum_{n=1}^{\infty} W_{smn}\Phi_{sm}(x)\,\Psi_{sn}(y)e^{i\omega_n t} \tag{30}$$

where (W_{bmn}, W_{smn}) are the unknown coefficients and the functions Φ_m and Ψ_n satisfy boundary conditions. Boundary conditions based on the present plate model are:

$$\begin{aligned} w_b = w_s = 0,\ \frac{\partial^2 w_b}{\partial x^2} = \frac{\partial^2 w_s}{\partial x^2} = \frac{\partial^2 w_b}{\partial y^2} \\ = \frac{\partial^2 w_s}{\partial y^2} = 0 \text{ simply} - \text{supported edge} \end{aligned} \tag{31}$$

$$w_b = w_s = 0,\ \frac{\partial w_b}{\partial x} = \frac{\partial w_s}{\partial x} = \frac{\partial w_b}{\partial y} = \frac{\partial w_s}{\partial y} = 0 \text{ clamped edge} \tag{32}$$

Inserting equations (29) and (30) into equations (27)–(28) and multiplying both sides of the equations by $\Phi_{im}\Psi_{in}\,(i = b, s)$ and integrating over the whole region leads to the following simultaneous equations as:

$$\begin{aligned}
&\int_0^b\int_0^a \Phi_{bm}\Psi_{bn}\Bigg[-D_{11}\Bigg[\frac{\partial^4\Phi_{bm}}{\partial x^4}\Psi_{bn} \\
&-\lambda\left(\frac{\partial^6\Phi_{bm}}{\partial x^6}\Psi_{bn} + \frac{\partial^4\Phi_{bm}}{\partial x^4}\frac{\partial^2\Psi_{bn}}{\partial y^2}\right)\Bigg] \\
&-2(D_{12}+2D_{66})\Bigg[\frac{\partial^2\Phi_{bm}}{\partial x^2}\frac{\partial^2\Psi_{bn}}{\partial y^2} \\
&-\lambda\left(\frac{\partial^4\Phi_{bm}}{\partial x^4}\frac{\partial^2\Psi_{bn}}{\partial y^2} + \frac{\partial^2\Phi_{bm}}{\partial x^2}\frac{\partial^4\Psi_{bn}}{\partial y^4}\right)\Bigg] \\
&-D_{22}\Bigg[\frac{\partial^4\Psi_{bm}}{\partial y^4}\Phi_{bn} - \lambda\left(\frac{\partial^6\Psi_{bm}}{\partial y^6}\Phi_{bn} + \frac{\partial^2\Phi_{bm}}{\partial x^2}\frac{\partial^4\Psi_{bn}}{\partial y^4}\right)\Bigg] \\
&-D_{11}^s\Bigg[\frac{\partial^4\Phi_{sm}}{\partial x^4}\Psi_{sn} - \lambda\left(\frac{\partial^6\Phi_{sm}}{\partial x^6}\Psi_{sn} + \frac{\partial^4\Phi_{sm}}{\partial x^4}\frac{\partial^2\Psi_{sn}}{\partial y^2}\right)\Bigg] \\
&-2(D_{12}^s+2D_{66}^s)\Bigg[\frac{\partial^2\Phi_{sm}}{\partial x^2}\frac{\partial^2\Psi_{sn}}{\partial y^2} - \lambda\Bigg(\frac{\partial^4\Phi_{sm}}{\partial x^4}\frac{\partial^2\Psi_{sn}}{\partial y^2} \\
&+\frac{\partial^2\Phi_{sm}}{\partial x^2}\frac{\partial^4\Psi_{sn}}{\partial y^4}\Bigg)\Bigg] - D_{22}^s\Bigg[\frac{\partial^4\Psi_{sm}}{\partial y^4}\Phi_{sn} \\
&-\lambda\left(\frac{\partial^6\Psi_{sm}}{\partial y^6}\Phi_{sn} + \frac{\partial^2\Phi_{sm}}{\partial x^2}\frac{\partial^4\Psi_{sn}}{\partial y^4}\right)\Bigg] \\
&+I_0\omega^2\Bigg[(\Phi_{bm}\Psi_{bn}+\Phi_{sm}\Psi_{sn}) - \mu\Bigg(\frac{\partial^2\Phi_{bm}}{\partial x^2}\Psi_{bn} \\
&+\frac{\partial^2\Phi_{sm}}{\partial x^2}\Psi_{sn} + \frac{\partial^2\Psi_{sm}}{\partial y^2}\Phi_{sn} + \frac{\partial^2\Psi_{bm}}{\partial y^2}\Phi_{bn}\Bigg)\Bigg] \\
&-I_2\omega^2\Bigg[\frac{\partial^2\Phi_{bm}}{\partial x^2}\Psi_{bn} + \frac{\partial^2\Psi_{bm}}{\partial y^2}\Phi_{bn} - \mu\Bigg(\frac{\partial^4\Phi_{bm}}{\partial x^4}\Psi_{bn} \\
&+2\frac{\partial^2\Phi_{bm}}{\partial x^2}\frac{\partial^2\Psi_{bn}}{\partial y^2} + \frac{\partial^b\Psi_{sm}}{\partial y^4}\Phi_{bn}\Bigg)\Bigg] \\
&-J_2\omega^2\Bigg[\frac{\partial^2\Phi_{sm}}{\partial x^2}\Psi_{sn} + \frac{\partial^2\Psi_{sm}}{\partial y^2}\Phi_{sn} - \mu\Bigg(\frac{\partial^4\Phi_{sm}}{\partial x^4}\Psi_{sn} \\
&+2\frac{\partial^2\Phi_{sm}}{\partial x^2}\frac{\partial^2\Psi_{sn}}{\partial y^2} + \frac{\partial^4\Psi_{sm}}{\partial y^4}\Phi_{sn}\Bigg)\Bigg] \\
&-N_x^0(y)\Bigg[1-\mu\left(\frac{\partial^2}{\partial x^2}+\frac{\partial^2}{\partial y^2}\right)\Bigg] \\
&\times\left[\frac{\partial^2\Phi_{bm}}{\partial x^2}\Psi_{bn} + \frac{\partial^2\Phi_{sm}}{\partial x^2}\Psi_{sn}\right] \\
&-N_y^0(x)\Bigg[1-\mu\left(\frac{\partial^2}{\partial x^2}+\frac{\partial^2}{\partial y^2}\right)\Bigg] \\
&\times\left[\frac{\partial^2\Psi_{sm}}{\partial y^2}\Phi_{sn} + \frac{\partial^2\Psi_{bm}}{\partial y^2}\Phi_{bn}\right] \\
&+k_p\left(1-\mu\left(\frac{\partial}{\partial x^2}+\frac{\partial}{\partial x^2}\right)\right)\Bigg[\Bigg(\frac{\partial^2\Phi_{bm}}{\partial x^2}\Psi_{bn} \\
&+\frac{\partial^2\Phi_{sm}}{\partial x^2}\Psi_{sn} + \frac{\partial^2\Psi_{sm}}{\partial y^2}\Phi_{sn} + \frac{\partial^2\Psi_{bm}}{\partial y^2}\Phi_{bn}\Bigg)\Bigg] \\
&-k_w\left(1-\mu\left(\frac{\partial}{\partial x^2}+\frac{\partial}{\partial x^2}\right)\right) \\
&\times(\Phi_{bm}\Psi_{bn}+\Phi_{sm}\Psi_{sn})]\mathrm{d}x\,\mathrm{d}y = 0
\end{aligned} \tag{33}$$

$$\begin{aligned}
&\int_0^b\int_0^a \Phi_{sm}\Psi_{sn}\Bigg[-D_{11}^s\Bigg[\frac{\partial^4\Phi_{bm}}{\partial x^4}\Psi_{bn} \\
&-\lambda\left(\frac{\partial^6\Phi_{bm}}{\partial x^6}\Psi_{bn} + \frac{\partial^4\Phi_{bm}}{\partial x^4}\frac{\partial^2\Psi_{bn}}{\partial y^2}\right)\Bigg] \\
&-2(D_{12}^s+2D_{66}^s)\Bigg[\frac{\partial^2\Phi_{bm}}{\partial x^2}\frac{\partial^2\Psi_{bn}}{\partial y^2} \\
&-\lambda\left(\frac{\partial^4\Phi_{bm}}{\partial x^4}\frac{\partial^2\Psi_{bn}}{\partial y^2} + \frac{\partial^2\Phi_{bm}}{\partial x^2}\frac{\partial^4\Psi_{bn}}{\partial y^4}\right)\Bigg] \\
&-D_{22}^s\Bigg[\frac{\partial^4\Psi_{bm}}{\partial y^4}\Phi_{bn} - \lambda\left(\frac{\partial^6\Psi_{bm}}{\partial y^6}\Phi_{bn} + \frac{\partial^2\Phi_{bm}}{\partial x^2}\frac{\partial^4\Psi_{bn}}{\partial y^4}\right)\Bigg] \\
&-H_{11}^s\Bigg[\frac{\partial^4\Phi_{sm}}{\partial x^4}\Psi_{sn} - \lambda\left(\frac{\partial^6\Phi_{sm}}{\partial x^6}\Psi_{sn} + \frac{\partial^4\Phi_{sm}}{\partial x^4}\frac{\partial^2\Psi_{sn}}{\partial y^2}\right)\Bigg] \\
&-2(H_{12}^s+2H_{66}^s)\Bigg[\frac{\partial^2\Phi_{sm}}{\partial x^2}\frac{\partial^2\Psi_{sn}}{\partial y^2} - \lambda\Bigg(\frac{\partial^4\Phi_{sm}}{\partial x^4}\frac{\partial^2\Psi_{sn}}{\partial y^2} \\
&+\frac{\partial^2\Phi_{sm}}{\partial x^2}\frac{\partial^4\Psi_{sn}}{\partial y^4}\Bigg)\Bigg] - H_{22}^s\Bigg[\frac{\partial^4\Psi_{sm}}{\partial y^4}\Phi_{sn} \\
&-\lambda\left(\frac{\partial^6\Psi_{sm}}{\partial y^6}\Phi_{sn} + \frac{\partial^2\Phi_{sm}}{\partial x^2}\frac{\partial^4\Psi_{sn}}{\partial y^4}\right)\Bigg] + I_0\omega^2[\Phi_{bm}\Psi_{bn} \\
&-\mu\left(\frac{\partial^2\Phi_{bm}}{\partial x^2}\Psi_{bn} + \frac{\partial^2\Phi_{sm}}{\partial x^2}\Psi_{sn} + \frac{\partial^2\Psi_{sm}}{\partial y^2}\Phi_{sn}\right. \\
&\left.+\frac{\partial^2\Psi_{bm}}{\partial y^2}\Phi_{bn}\right)\Bigg] - J_2\omega^2\Bigg[\frac{\partial^2\Phi_{bm}}{\partial x^2}\Psi_{bn} + \frac{\partial^2\Psi_{bm}}{\partial y^2}\Phi_{bn} \\
&-\mu\left(\frac{\partial^4\Phi_{bm}}{\partial x^4}\Psi_{bn} + 2\frac{\partial^2\Phi_{bm}}{\partial x^2}\frac{\partial^2\Psi_{bn}}{\partial y^2}\right.
\end{aligned}$$

$$
\begin{aligned}
&+\frac{\partial^b \Psi_{sm}}{\partial y^4}\Phi_{bn}\Big)\Big]-K_2\omega^2\Big[\frac{\partial^2\Phi_{sm}}{\partial x^2}\Psi_{sn}\\
&+\frac{\partial^2\Psi_{sm}}{\partial y^2}\Phi_{sn}-\mu\Big(\frac{\partial^4\Phi_{sm}}{\partial x^4}\Psi_{sn}\\
&+2\frac{\partial^2\Phi_{sm}}{\partial x^2}\frac{\partial^2\Psi_{sn}}{\partial y^2}+\frac{\partial^4\Psi_{sm}}{\partial y^4}\Phi_{sn}\Big)\Big]\\
&-N_x^0(y)\Big[1-\mu\Big(\frac{\partial^2}{\partial x^2}+\frac{\partial^2}{\partial y^2}\Big)\Big]\Big[\frac{\partial^2\Phi_{bm}}{\partial x^2}\Psi_{bn}+\frac{\partial^2\Phi_{sm}}{\partial x^2}\Psi_{sn}\Big]\\
&-N_y^0(x)\Big[1-\mu\Big(\frac{\partial^2}{\partial x^2}+\frac{\partial^2}{\partial y^2}\Big)\Big]\Big[\frac{\partial^2\Psi_{sm}}{\partial y^2}\Phi_{sn}+\frac{\partial^2\Psi_{bm}}{\partial y^2}\Phi_{bn}\Big]\\
&+A_{55}^s\Big[\frac{\partial^2\Phi_{sm}}{\partial x^2}\Psi_{sn}-\lambda\Big(\frac{\partial^4\Phi_{sm}}{\partial x^4}\Psi_{sn}+\frac{\partial^2\Phi_{sm}}{\partial x^2}\frac{\partial^2\Psi_{sn}}{\partial y^2}\Big)\Big]\\
&+A_{44}^s\Big[\frac{\partial^2\Psi_{sm}}{\partial y^2}\Phi_{sn}-\lambda\Big(\frac{\partial^4\Psi_{sm}}{\partial y^4}\Phi_{sn}+\frac{\partial^2\Phi_{sm}}{\partial x^2}\frac{\partial^2\Psi_{sn}}{\partial y^2}\Big)\\
&+k_p\Big(1-\mu\Big(\frac{\partial}{\partial x^2}+\frac{\partial}{\partial x^2}\Big)\Big)\Big[\frac{\partial^2\Phi_{bm}}{\partial x^2}\Psi_{bn}\\
&+\frac{\partial^2\Phi_{sm}}{\partial x^2}\Psi_{sn}+\frac{\partial^2\Psi_{sm}}{\partial y^2}\Phi_{sn}+\frac{\partial^2\Psi_{bm}}{\partial y^2}\Phi_{bn}\Big)\Big]\\
&-k_w\Big(1-\mu\Big(\frac{\partial}{\partial x^2}+\frac{\partial}{\partial x^2}\Big)\Big)(\Phi_{bm}\Psi_{bn}+\Phi_{sm}\Psi_{sn})\Big]\\
&\times dx\,dy=0
\end{aligned}
\tag{34}
$$

The function Φ_m for different boundary conditions is defined by:

$$
\begin{aligned}
\text{SS}:\ \Phi_m(x)&=\sin(\lambda_m x)\\
\lambda_m&=\frac{m\pi}{a}
\end{aligned}
\tag{35}
$$

$$
\begin{aligned}
\text{CC}:\ \Phi_m(x)&=\sin(\lambda_m x)-\sinh(\lambda_m x)\\
&\quad-\xi_m(\cos(\lambda_m x)-\cosh(\lambda_m x))\\
\xi_m&=\frac{\sin(\lambda_m x)-\sinh(\lambda_m x)}{\cos(\lambda_m x)-\cosh(\lambda_m x)}\\
\lambda_1&=4.730,\lambda_2=7.853,\lambda_3=10.996,\\
\lambda_4&=14.137,\quad \lambda_{m\geq 5}=\frac{(m+0.5)\pi}{a}
\end{aligned}
\tag{36}
$$

The function Ψ_n can be obtained by replacing x, m and a, respectively by y, n and b. Setting the coefficient matrix of the above equations leads to the following eigenvalue problem:

$$
([K]+\omega^2[M])\begin{Bmatrix} W_b \\ W_s \end{Bmatrix}=0 \tag{37}
$$

where [M] and [K] are the mass matrix and stiffness matrix, respectively. Finally, setting the coefficient matrix to zero gives the natural frequencies. It should be noted that calculations are performed based on the following dimensionless quantities:

$$
\begin{aligned}
&\hat{\omega}=\omega\frac{\mathrm{a}^2}{h}\sqrt{\frac{\rho}{\mathrm{E}}},\ K_w=\mathrm{k}_w\frac{\mathrm{a}^4}{D^*},\ K_p=\mathrm{k}_p\frac{\mathrm{a}^2}{D^*},\\
&D^*=\frac{Eh^3}{12(1-\nu^2)},\ \bar{N}=N\frac{\mathrm{a}^2}{D^*}
\end{aligned}
\tag{38}
$$

4. Numerical results and discussions

This section is devoted to study the vibration behavior of nonlocal strain gradient graphene sheets on elastic substrate under in-plane nonuniform loads based on a two-variable shear deformation theory. The model introduces two scale coefficients related to nonlocal and strain gradient effects for more accurate analysis of graphene sheets. Material properties of the graphene sheet are: $E=1$ TPa, $\nu=0.19$ and $\rho=2300\,\mathrm{kg/m^3}$. Also, thickness of the graphene sheet is considered as $\mathrm{h}=0.34$ nm. The configuration of graphene sheet under in-plane loads is presented in Figures 1 and 2. Natural frequencies of graphene sheet are first validated with those of molecular dynamics obtained by Ansari et al. (2010). Results for different lengths of graphene sheet are presented in Table 1 and a good agreement is observed. In Table 1, it is assumed that the graphene sheet is square and the nonlocal parameter is considered as $\mu^2=1.34\ \mathrm{nm}^2$. Natural frequencies of a graphene sheet are validated with those obtained by Sobhy (2014) for various nonlocal parameters ($\mu=0$, 1, 2, 3, 4 nm^2) and foundation constants ($\{K_w, K_p\}=\{(0,0), (100,0), (0,20)\}$. Obtained frequencies via the present Galerkin method are in excellent agreement with those of the exact solution presented by Sobhy (2014), as tabulated in Table 2. For comparison study, the strain gradient or length scale parameter is set to zero ($\lambda=0$).

Examination of nonlocal and strain gradient effects on vibration frequencies of graphene sheets with respect to uniaxial dimensionless load is presented in Figure 3 when $a/h=10$. It is clear that when $\lambda=0$, the natural frequencies of a graphene sheet based on the well-known nonlocal elasticity theory will be obtained. However, when both $\mu=0$ and $\lambda=0$, the results based on classical continuum mechanics are rendered. It is observed that natural frequency of graphene sheet reduces by inclusion of nonlocal parameter at a fixed value of in-plane load. This observation indicates that the nonlocal parameter exerts a stiffness-softening effect which leads to lower vibration frequencies. But, effect of the nonlocal parameter on the magnitude of natural frequencies depends on the strain gradient or length scale parameter. In fact, the natural frequency of a graphene sheet increases with increase of

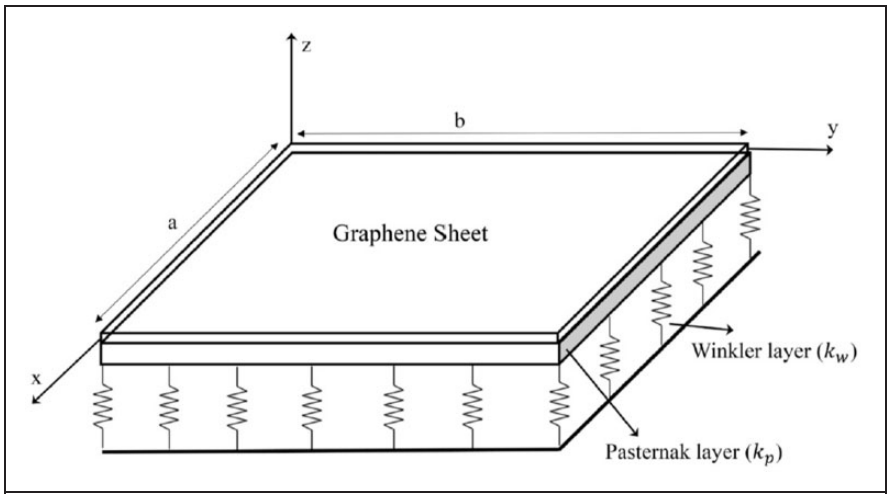

Figure 1. Configuration of the grapheme sheet resting on the elastic substrate.

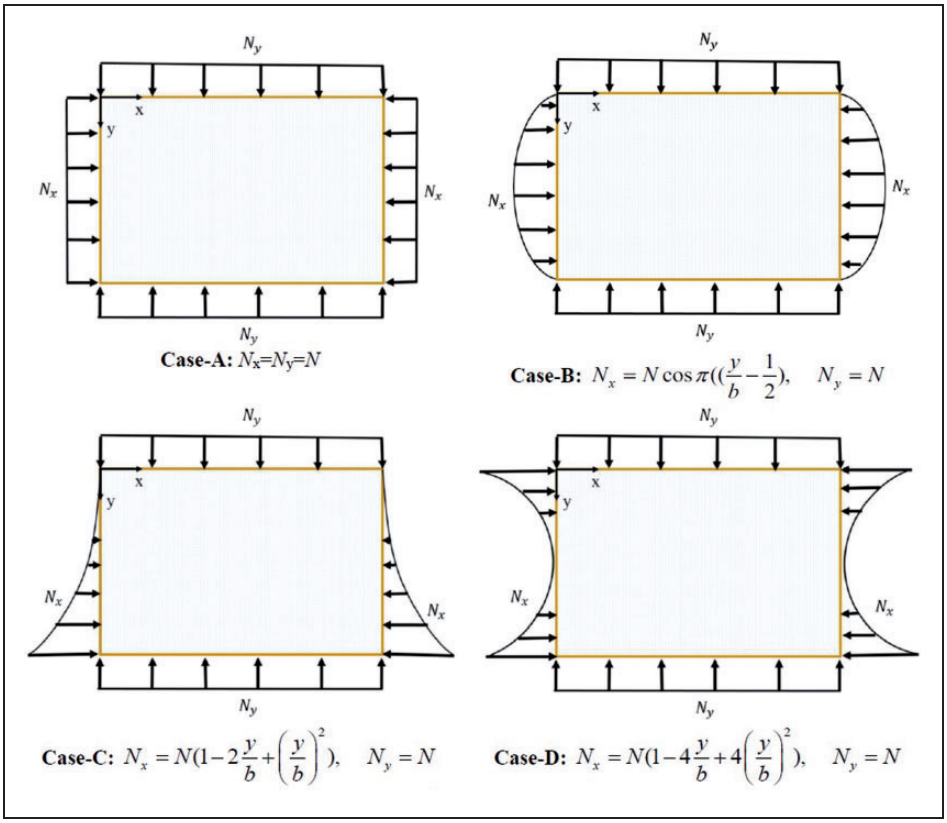

Figure 2. Different cases of in-plane bending loads.

the length scale parameter which highlights the stiffness-hardening effect due to the strain gradients. It should be pointed out that increase of dimensionless load degrades the plate stiffness and natural frequencies reduce until a critical point in which the frequencies become zero. At this point, the graphene sheet buckles and does not oscillate. However, obtained critical loads depend on the length scale parameter. In fact, inclusion of the length scale parameter in nonlocal strain gradient theory leads to higher critical

buckling loads compared with nonlocal theory. So, it can be concluded that critical buckling loads obtained by nonlocal elasticity theory are underestimated. As a consequence, it is very important to consider both nonlocal and length scale parameters in analysis of graphene sheets.

Table 1. Comparison of natural frequency of a graphene sheet with molecular dynamics (MD) simulation ($a/b = 1$, $\mu^2 = 1.34$ nm^2).

a (nm)	MD simulation	Present study
10	0.0595014	0.05926
15	0.0277928	0.02816
20	0.0158141	0.01624
25	0.0099975	0.01063
30	0.0070712	0.00731

Figure 4 shows the variation of dimensionless frequency of nonlocal strain gradient graphene sheets with respect to dimensionless load for different cases of in-plane loads when $a/h = 10$, $\mu = 1$ nm^2 and $\lambda = 0.5$ nm^2. Case-A and case-B are in-plane uniform and sinusoidal loads, respectively. Also, case-C and case-D are corresponding to the in-plane parabolic loads. It is clear that the in-plane bending load degrades the plate stiffness and affect significantly the performance of structures. Maximum and minimum buckling loads are obtained when the graphene sheet is subjected to case-D and case-B loads, respectively. In fact, sinusoidal in-plane load (case-B) has largest resultant near the middle surface of the graphene sheet. But, parabolic in-plane load (case-D) has smallest resultant leading to larger critical buckling loads. It is also clear that

Table 2. Comparison of natural frequency of a graphene sheet for various nonlocal and foundation parameters ($a/h = 10$).

	$K_w = 0$, $K_p = 0$		$K_w = 100$, $K_p = 0$		$K_w = 0$, $K_p = 20$	
μ	Sobhy (2014)	Present study	Sobhy (2014)	Present study	Sobhy (2014)	Present study
0	1.93861	1.93861	2.18396	2.18396	2.7841	2.78410
1	1.17816	1.17816	1.54903	1.54903	2.31969	2.31969
2	0.92261	0.92261	1.36479	1.36479	2.20092	2.20092
3	0.78347	0.78347	1.27485	1.27485	2.14629	2.14629
4	0.69279	0.69279	1.22122	1.22122	2.11486	2.11486

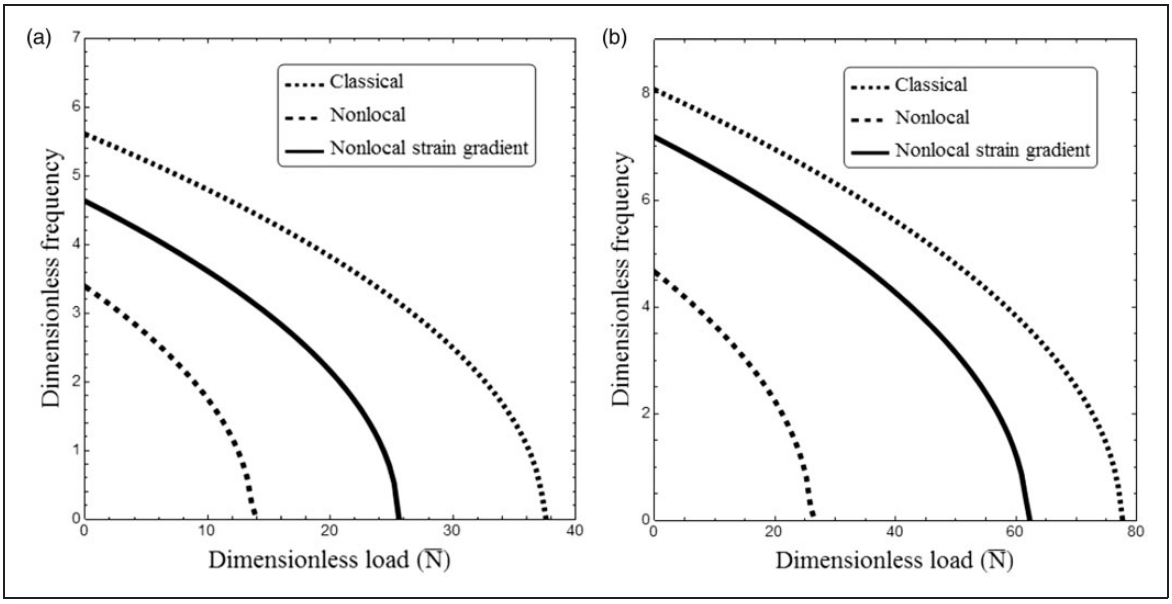

Figure 3. Variation of dimensionless frequency versus dimensionless uniaxial uniform load for different elasticity theories ($a/h = 10$, $\mu = 1$nm^2, and $\lambda = 0.5$ nm^2): (a) SSSS, (b) SSCC.

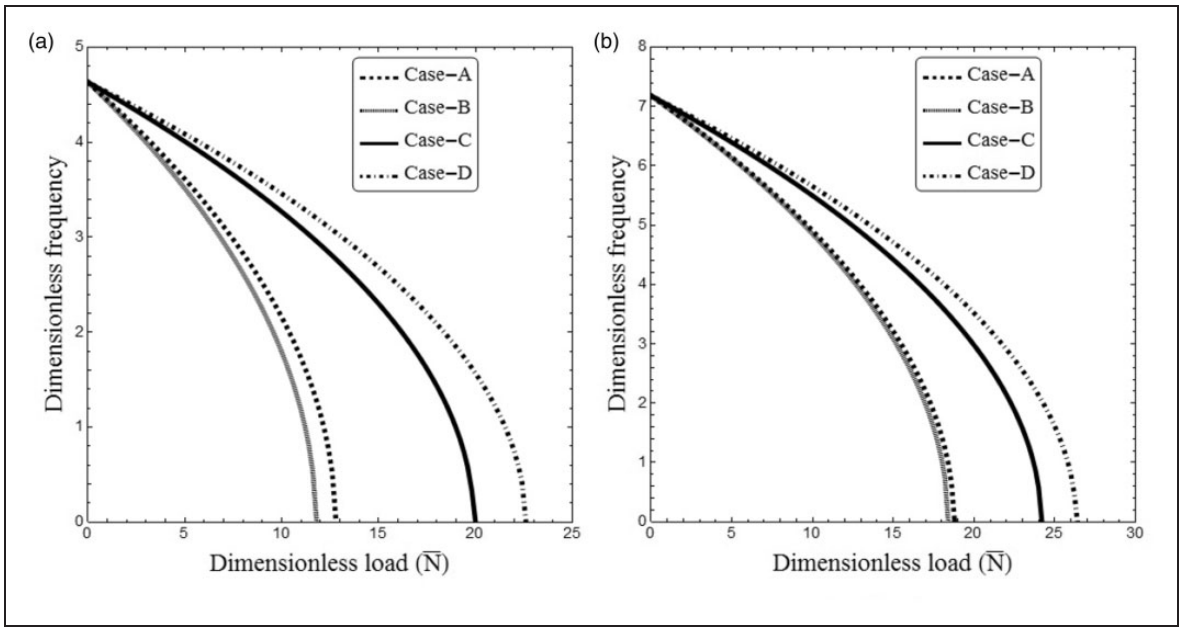

Figure 4. Variation of dimensionless frequency versus dimensionless load for different cases of edge loading ($a/h = 10$, $\mu = 1$ nm^2, and $\lambda = 0.5$ nm^2): (a) SSSS, (b) SSCC.

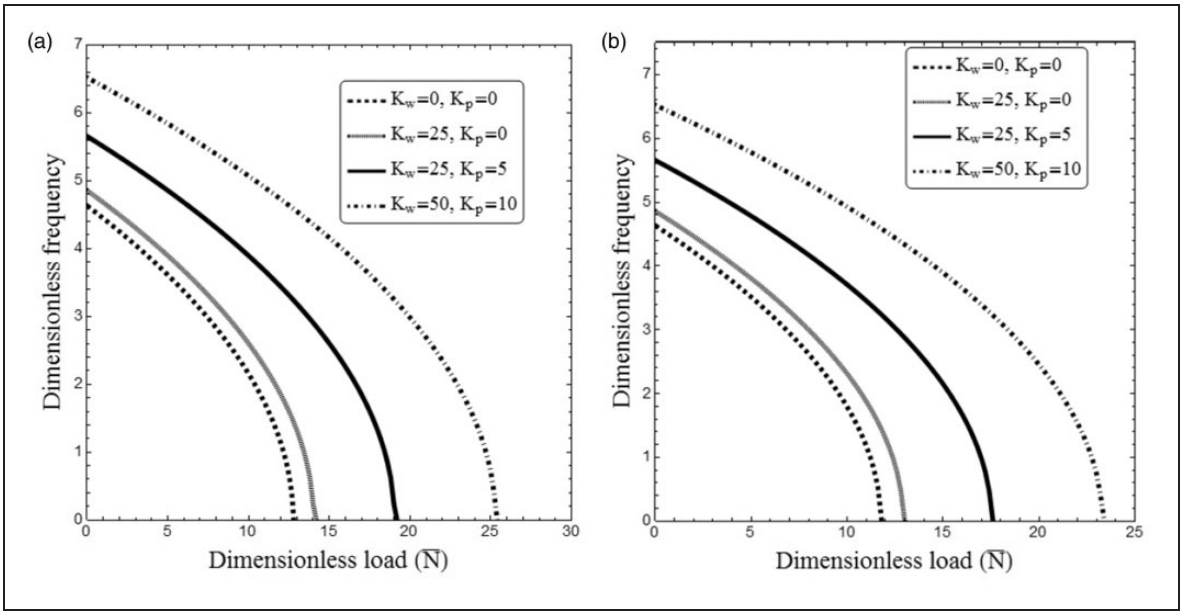

Figure 5. Variation of dimensionless frequency versus dimensionless load for different formulation parameters ($a/h = 10$, $\mu = 1$ nm^2, and $\lambda = 0.5$ nm^2): (a) Case-A, (b) Case-B.

making the graphene sheet more rigid by increasing the number of clamped edges leads to higher natural frequencies. Therefore, the SSCC boundary condition gives larger buckling loads compared with SSSS one for all types of loadings.

Effect of the Winkler–Pasternak foundation on vibration frequencies of nonlocal strain gradient graphene sheets is plotted in Figure 5 at $a/h = 10$, $\mu = 1$ nm^2, and $\lambda = 0.5$ nm^2. It is clear that vibration behavior of the graphene sheet depends on the values of both Winkler and Pasternak parameters. In fact, the Pasternak layer provides a continuous interaction with the graphene sheet, while the Winkler layer has a discontinuous interaction with the graphene sheet.

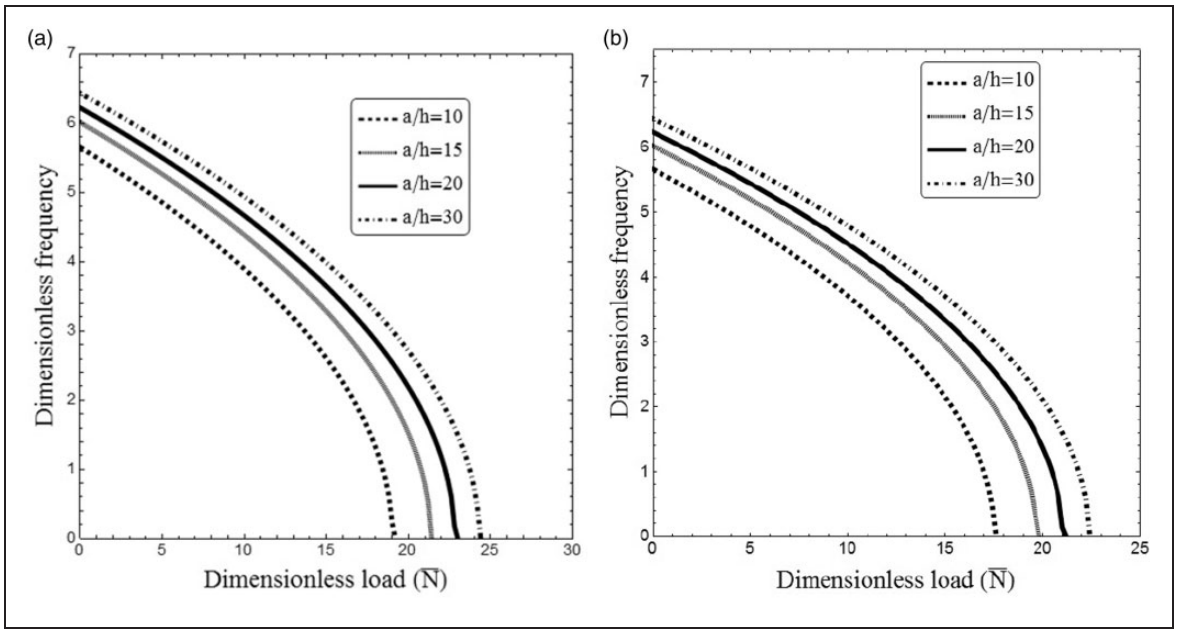

Figure 6. Variation of dimensionless frequency versus dimensionless load for different side-to-side thickness ratios ($K_w = 25$, $K_p = 5$, $\mu = 1$ nm^2, and $\lambda = 0.5$ nm^2): (a) Case-A, (b) Case-B.

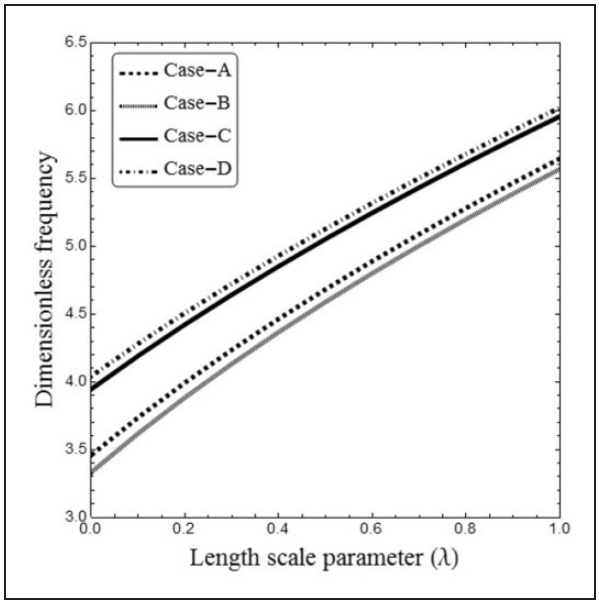

Figure 7. Variation of dimensionless frequency versus length scale parameter for different edge loadings ($K_w = 25$, $K_p = 5$, $\mu = 1$ nm^2, and $N = 6$).

Increasing Winkler and Pasternak parameters leads to larger frequencies by enhancing the bending rigidity of the graphene sheets. But, the Pasternak layer shows more increasing effect on natural frequencies compared with the Winkler layer. It is found that increasing foundation parameters yields larger critical buckling loads. In fact, higher values of foundation parameters lead to postponement in buckling of graphene sheets.

Figure 6 depicts the variation of dimensionless frequency versus dimensionless in-plane load for different side-to-thickness ratios (a/h) at $K_w = 25$, $K_p = 5$, $\mu = 1$ nm^2, and $\lambda = 0.5$ nm^2. In Figure 6, uniform and sinusoidal in-plane loads are considered. It is seen that graphene sheets with higher side-to-thickness ratios have larger vibration frequencies. Accordingly, graphene sheets with higher side-to-thickness ratios have a higher critical buckling load.

Effect of loading type on the variation of dimensionless frequency of graphene sheets with respect to the length scale parameter is plotted in Figure 7 when $N = 6$, $K_w = 25$, $K_p = 5$, and $\mu = 1$ nm^2. As the resultant of in-plane load increases, effect of applied load in x direction becomes more important. This leads to a significant decrease in plate stiffness and natural frequencies. At a fixed length scale parameter, obtained frequencies by different loadings obey the following form: case-D > case-C > case-A > case-B. Also, for all types of loading, increase of length scale parameter leads to enlargement of the natural frequency of the graphene sheet. This is due to a significant increment in plate stiffness by the strain gradient effect.

5. Conclusions

In this paper, nonlocal strain gradient theory is employed to investigate free vibration behavior of single-layer graphene sheets under in-plane

nonuniform loads resting on elastic medium using a refined two-variable plate theory. The theory introduces two scale parameters corresponding to nonlocal and strain gradient effects to capture both stiffness-softening and stiffness-hardening influences. Hamilton's principle is employed to obtain the governing equation of a nonlocal strain gradient graphene sheet. These equations are solved via Galerkin's method to obtain the natural frequencies. It is observed that the natural frequency of the graphene sheet reduces with increase of the nonlocal parameter. In contrast, natural frequency increases with increase of the length scale parameter which highlights the stiffness-hardening effect due to the strain gradients. Also, increase of temperature degrades the plate stiffness and natural frequencies reduce until a critical point in which the frequencies become zero. It is seen that nonlocal strain gradient theory provides larger critical buckling loads than nonlocal elasticity theory. In fact, considering strain gradient effects leads to postponement in buckling of the grapheme sheets. Also, when the in-plane load resultant reduces, vibration frequencies will increase.

Declaration of Conflicting Interests

The authors declared no potential conflicts of interest with respect to the research, authorship, and/or publication of this article.

Funding

The authors received no financial support for the research, authorship, and/or publication of this article.

References

Aksencer T and Aydogdu M (2011) Levy type solution method for vibration and buckling of nanoplates using nonlocal elasticity theory. *Physica E: Low-dimensional Systems and Nanostructures* 43(4): 954–959.

Ansari R, Sahmani S and Arash B (2010) Nonlocal plate model for free vibrations of single-layered graphene sheets. *Physics Letters A* 375(1): 53–62.

Ansari R, Arash B and Rouhi H (2011) Vibration characteristics of embedded multi-layered graphene sheets with different boundary conditions via nonlocal elasticity. *Composite Structures* 93(9): 2419–2429.

Ansari R, Shojaei MF and Gholami R (2016) Size-dependent nonlinear mechanical behavior of third-order shear deformable functionally graded microbeams using the variational differential quadrature method. *Composite Structures* 136(2): 669–683.

Ansari R and Sahmani S (2013) Prediction of biaxial buckling behavior of single-layered graphene sheets based on nonlocal plate models and molecular dynamics simulations. *Applied Mathematical Modelling* 37(12): 7338–7351.

Arani AG, Haghparast E and Zarei HB (2016) Nonlocal vibration of axially moving graphene sheet resting on orthotropic visco-Pasternak foundation under longitudinal magnetic field. *Physica B: Condensed Matter* 495(1): 35–49.

Bessaim A, Houari MSA, Bernard F, et al. (2015) A nonlocal quasi-3D trigonometric plate model for free vibration behaviour of micro/nanoscale plates. *Structural Engineering and Mechanics* 56(2): 223–240.

Ebrahimi F and Barati MR (2016a) Vibration analysis of nonlocal beams made of functionally graded material in thermal environment. *The European Physical Journal Plus* 131(8): 279–290.

Ebrahimi F and Barati MR (2016b) A unified formulation for dynamic analysis of nonlocal heterogeneous nanobeams in hygro-thermal environment. *Applied Physics A* 122(9): 792–800.

Ebrahimi F and Barati MR (2016c) Hygrothermal buckling analysis of magnetically actuated embedded higher order functionally graded nanoscale beams considering the neutral surface position. *Journal of Thermal Stresses* 39(10): 1210–1229.

Ebrahimi F and Barati MR (2016d) Vibration analysis of smart piezoelectrically actuated nanobeams subjected to magneto-electrical field in thermal environment. *Journal of Vibration and Control* E-pub before print. doi/abs/10.1177/1077546316646239.

Ebrahimi F and Barati MR (2016e) Wave propagation analysis of quasi-3D FG nanobeams in thermal environment based on nonlocal strain gradient theory. *Applied Physics A* 122(9): 843–860.

Ebrahimi F and Barati MR (2016f) Size-dependent dynamic modeling of inhomogeneous curved nanobeams embedded in elastic medium based on nonlocal strain gradient theory. *Proceedings of the Institution of Mechanical Engineers, Part C: Journal of Mechanical Engineering Science* 0954406216668912.

Ebrahimi F and Barati MR (2017a) Hygrothermal effects on vibration characteristics of viscoelastic FG nanobeams based on nonlocal strain gradient theory. *Composite Structures* 159(1): 433–444.

Ebrahimi F and Barati MR (2017b) A nonlocal strain gradient refined beam model for buckling analysis of size-dependent shear-deformable curved FG nanobeams. *Composite Structures* 159(1): 174–182.

Ebrahimi F, Barati MR and Dabbagh A (2016) A nonlocal strain gradient theory for wave propagation analysis in temperature-dependent inhomogeneous nanoplates. *International Journal of Engineering Science* 107(10): 169–182.

Eringen AC (1983) On differential equations of nonlocal elasticity and solutions of screw dislocation and surface waves. *Journal of Applied Physics* 54(9): 4703–4710.

Eringen AC and Edelen DGB (1972) On nonlocal elasticity. *International Journal of Engineering Science* 10(3): 233–248.

Farajpour A, Shahidi AR, Mohammadi M, et al. (2012) Buckling of orthotropic micro/nanoscale plates under linearly varying in-plane load via nonlocal continuum mechanics. *Composite Structures* 94(5): 1605–1615.

Hashemi SH, Mehrabani H and Ahmadi-Savadkoohi A (2015) Exact solution for free vibration of coupled double